NATURAL SCIENCE REVIEW 3 200702 (2026)
nsr.jinr.int

Structural, magnetic states and pressure-induced phenomena in complex nanosized magnetic oxides

D. P. Kozlenko*[1], N. M. Belozerova[1,2], S. E. Kichanov[1], E. V. Lukin[1], O. N. Lis†[1], A. V. Rutkauskas[1], B. N. Savenko[1], Z. Jirák[3], G. S. Rymski[4], A. L. Zhaludkevich[4], and N. T. Dang[5]

[1] *Joint Institute for Nuclear Research, 141980, Dubna, Russia*
[2] *Centre for Photonics and 2D Materials, Moscow Institute of Physics and Technology, 141701, Dolgoprudny, Russia*
[3] *Institute of Physics, CAS, Cukrovarnická 10, 162 00 Praha 6, Czech Republic*
[4] *Scientific-Practical Materials Research Centre of the National Academy of Sciences of Belarus, 220072, Minsk, Belarus*
[5] *Institute of Research and Development, Duy Tan University, 550000 Danang, Vietnam*

Abstract

The results of the recent investigations of the crystal and magnetic structure of complex nanosized manganese and iron oxides using neutron diffraction, X-ray diffraction and other techniques over a wide range of thermodynamic parameters (temperature and pressure) are considered. In the nanostructured manganites $La_{1-x}Sr_xMnO_3$ ($x = 0.28-0.47$), the coexistence of the ferromagnetic (FM) and A-type antiferromagnetic (AFM) states has been evidenced, implying the production of core-shell nanoparticles with distinctive structural and magnetic properties of ordering of internal and external components. Application of high pressure significantly modifies the ratio of FM and AFM components. For the nanostructured $Zn_{0.34}Fe_{2.53}O_4$ ferrite, a distribution of Zn and Fe atoms in the crystal structure, as well as the parameters of crystal and magnetic structures, have been estimated. The oxygen vacancies were detected and their amount was estimated. The gradual transition of the structural phase from the initial cubic spinel phase to the orthorhombic post-spinel phase was observed at high pressures in this material, relevant to $CoFe_2O_4$ ferrite. In the latter case, the phase transition is also accompanied by suppression of the ordered magnetic moments. Surprisingly, in the most cases, the properties of structural and magnetic states of the studied nanosized manganites and ferrites are notably different from those for the relevant bulk forms of these materials. The microscopic mechanisms responsible for this distinction have been discussed in detail.

Keywords: high pressure, neutron diffraction, manganites, ferrites, magnetic structure

DOI: 10.54546/NaturalSciRev.200702

*Corresponding author e-mail address: denk@nf.jinr.ru
†Corresponding author e-mail address: lisa_9477@mail.ru

Received: 22 January 2026; Revised: 12 February 2026; Accepted: 13 February 2026; Published: 23 April 2026; Corrected: 24 April 2026 (the incorrect order of the authors and the affiliation of one of them were corrected)

1. Introduction

The achievements in condensed matter physics, materials science, and development of current technologies in recent decades have been inextricably interrelated with research of complex oxide materials [1]. The novel and challenging phenomena like high-temperature superconductivity [2], colossal magnetoresistance (CMR) [3–6], insulator–metal transitions [7, 8], charge and orbital ordering [8, 9], magnetoelectric effects [10], and spin crossover [11] have been discovered in such materials. Many of these physical phenomena have been basis for potential innovative technological applications [12], including development of components of the data registering and storage devices [13], electronics, communication, energy, etc. Figuring out microscopic effects of implementation of these phenomena is among the most urgent tasks of condensed matter research.

In the manganites $R_{1-x}A_xMnO_3$ (R — rare earth, A — alkaline earth elements) with the perovskite-like structure, most of the phenomena mentioned above have been observed (except for high-temperature superconductivity and spin crossover) [9, 11, 14] and these materials in the bulk form have been extensively explored in recent years. It is widely accepted that the delicate interplay between magnetic, transport and electronic properties in these systems is the result of a complicated balance between the ferromagnetic (FM) Mn^{3+}–O^{2-}–Mn^{4+} double exchange, mediated by charge carriers of the e_g nature, and the antiferromagnetic (AFM) Mn^{4+}–O^{2-}–Mn^{4+} or Mn^{3+}–O^{2-}–Mn^{3+} superexchange interactions between localized magnetic moments, coupled to lattice and orbital degrees of freedom [4, 7, 15–18]. This concept allows explaining the FM ordering, as well as various types of the AFM ordering, magnetic and electronic phase transitions in the doped manganites $R_{1-x}A_xMnO_3$ [7, 17, 19–26], depending on the concentration x, mediated by the content of Mn^{3+} and Mn^{4+} ions [3, 4, 6, 7].

At present, focus is on the hole-doped ($x < 0.5$) nanostructured manganites [18, 27–29]. The manganite nanoparticles have been promising for applications in biological research and biomedicine [30], in particular, for hyperthermia treatment [31]. In contrast to bulk materials, the crystal and magnetic structures of nanostructured manganese oxides display more complex properties [32–36]. There have been numerous reports on the size effect [33, 35] that makes the electrical and magnetic properties of manganese oxide nanoparticles different from those in bulk materials. Such as, the average magnetic moment of the manganese ion in nanostructured samples increases slightly as the nanoparticle size increases [33]. In nanoparticles of $La_{1-x}Sr_xMnO_3$ system for $x = 0.33$, a change in conductivity from metallic to insulating has been revealed upon variation of their size [37].

The ferrite compounds have also been the subject of particular research interest due to the intriguing magnetic phenomena arising from complex cation distributions at different crystallographic sites [38, 39]. Under ambient conditions, parent ferrite material, magnetite Fe_3O_4 [40], crystallizes in the structure of the inverse spinel with Fe^{3+} ions occupying A sites with a tetrahedral oxygen coordination and a mixture of Fe^{3+} and Fe^{2+} ions occupying B sites with an octahedral oxygen coordination in equal proportions [41]. The spins of the Fe ions at the A and B sublattices arrange ferrimagnetically below the Néel temperature $T_N = 850$ K. The chemical doping of both crystallographic sites often causes a redistribution of Fe^{3+} and Fe^{2+} ions between the tetrahedral and octahedral positions, which in turn affects the magnetic properties significantly. It should be emphasized that the zinc ferrite $ZnFe_2O_4$ has a spinel-type cubic structure at room temperature, typical for such materials [41, 42], while the copper ferrite $CuFe_2O_4$ has a tetragonal structure due to cooperative JT distortions driven by the distribution of Cu^{2+} ions into the octahedral B site [43]. The magnetic interaction J_{AB} between the magnetic moments of

iron positioned at the tetrahedral A and octahedral B sites is stronger than those between the moments of the ions in either tetrahedral sublattice J_{AA} or octahedral sublattice J_{BB} [41, 43]. All those magnetic interactions are antiferromagnetic, but the fact $|J_{AB}| \gg |J_{BB}| > |J_{AA}|$ provokes ferrimagnetism in Zn–Cu spinel ferrites compounds [43, 44], leaving the A–A and B–B couplings inherently frustrated. A substitution by diamagnetic ions suppresses the magnetic coupling J_{AB} and changes a balance between competing interactions J_{AA} and J_{BB}, giving prerequisites to forming the Yafet–Kittel triangular magnetic structure [45, 46]. A current scientific approach is the advanced synthesis of complex ferrites with controllable redistribution of iron ions between the A and B sites, resulting in the variation of a balance between complex magnetic interactions inside magnetic structure of ferrites [39, 43].

Similarly to manganites, nanostructured ferrites [47–49] present interesting fundamental issues arising from diversity of their structural and magnetic properties. A significant saturation magnetization [43, 48, 49], relatively high electrical resistivity [44, 50], low electrical losses, and good chemical stability make these materials important for a broad range of technological applications as components of transformer cores, radio frequency circuits, rod antennas, data storage and electronic devices, etc. [51–54]. Ferrite nanoparticles are promising materials for applications such as spin valves, magnetoresistive memories, medical diagnostics [47, 55], treatment and contrast agents for magnetic resonance imaging. In particular, it has been reported that surface vacancy defects [56, 57] can change the transport properties of nanostructured $ZnFe_2O_4$ ferrite from a semiconducting character to a metallic one [58]. As similar effect has also been observed in $MgFe_2O_4$ nanoparticles, where surface structural defects cause a change from a semiconducting state to a half-metallic one [59].

The variety of physical phenomena observed in nanostructured complex transition metal oxides is due to the strong correlation between spin, orbital, charge and lattice degrees of freedom. It results in serious difficulties in understanding the nature and mechanisms of these phenomena, especially at the microscopic level. Therefore, studying systems with strong correlations requires experimental approaches that allow for the separation of contributions from different interactions. A promising approach is a variation of thermodynamic parameters, such as high external pressure and temperature [60–68]. Estimating the microscopic mechanisms of the mediated relationship between the changes in the crystal and magnetic structure parameters is the cornerstone issue of this research area [69–74].

The neutron diffraction is the most suitable for this purpose, since it allows estimating both the crystal and magnetic structures of materials and provides more accurate estimation of the coordinates of light atoms compared to X-ray diffraction. In addition, high penetration of neutrons is advantageous for experiments with complex sample environments required for variation of pressure and temperature over a wide range. At the Frank Laboratory of Neutron Physics (FLNP) of the Joint Institute for Nuclear Research (JINR), two diffractometers, DN-12 and DN-6, have been constructed for structural investigations of materials at high pressures and low temperatures at the IBR-2 high-flux pulsed reactor. A long-lasting experience of experimental research in this area has been accumulated [75–80]. Here, we present an overview of recent results of neutron diffraction research of structural properties and magnetic states of nanostructured complex manganese and iron oxides [56, 80–88] that have been obtained at JINR through a long-term cooperation with scientific organizations from the present and former JINR Member States, including Belarus, the Czech Republic and Vietnam.

2. Materials and techniques

The details of manganites and spinel samples synthesis can be found in [81–86].

The neutron diffraction experiments were carried out in a pressure range up to 8 GPa and a temperature range of 5–290 K with the DN-6 and DN-12 diffractometers (the IBR-2 pulsed reactor, JINR, Dubna, Russia) [78–80]. The sapphire anvil high pressure cells were used [78]. The hemispherical holes were made at the centres of anvil culets to achieve the quasi-hydrostatic pressure distribution inside the cell. The sample with a volume of about 2 mm^3 was loaded into the aluminum gasket 0.8 mm thick positioneded between the anvils. The pressure was measured using the ruby fluorescence technique, with typical errors not exceeding 0.1 GPa. The diffraction patterns were accumulated at a scattering angle of 90° with the resolution $\Delta d/d = 0.02$. The special cryostat based on closed cycle helium refrigerator was used for providing low temperatures in high pressure experiments.

The nanoparticle size and morphology were characterized by transmission electron microscopy (TEM) on a Philips CM 120 instrument. Samples were taken from the final product after size fractionation but before surfactant removal, since thorough washing induces particle aggregation.

The primary phase analysis was carried out using X-ray diffraction at the PANanalytical Empyrean Advanced X-Ray Diffractometer in a Bragg–Brentano configuration with a Cu-Kα source and the PIXcel 3D detector. Generator settings for the tube were 40 kV and 4 mA. Scanning was carried out in the Bragg–Bentano geometry with an angle of scattering 2θ ranging from 20° to 100° in increments of 0.01°. The Oxford Cryosystems Phenix closed cycle cryostat was used for low temperature measurements between 15 and 300 K. The powder X-ray diffraction measurements at high pressures up to 40 GPa were implemented at the Xeuss 3.0 X-ray SAXS/WAXS instrument (Xenocs) with radiation generated by a GeniX3D source (Mo-Kα radiation, $\lambda = 0.71078$ Å), using an Eiger2 R 1M 2D-detector (Dectris). Both the PANalytical and Xeuss instruments are housed at the FLNP JINR.

The Raman spectra from nanostructured samples were accumulated using a LabRAM HR Evolution spectrometer (Horiba) with a wavelength excitation of 632.8 nm emitted using a He–Ne laser, 1800 grating, a confocal hole of 200 μm and ×20 objective.

The Boehler–Almax plate-type diamond anvil cell was used in the X-ray diffraction and Raman spectroscopy measurements. The sample was positioned in the hole 150 μm in diameter made in a Re gasket that was indented to about a 30-μm thickness. The 4:1 methanol–ethanol mixture was used as a pressure-transmitting environment. The pressure was also measured using the ruby fluorescence technique.

The neutron and X-ray diffraction data were analyzed using the software package FullProf [89–92].

3. Results

3.1. The phase separation in manganite nanoparticles

At the first stage, the crystal and magnetic structure of nanostructured hole-doped manganites $La_{1-x}Sr_xMnO_3$ (for $x = 0.28$ and 0.37) with different sizes of nanoparticles was studied in detail at ambient pressure [81, 82]. An average particle size was $d \sim 47$ nm for $La_{0.72}Sr_{0.28}MnO_3$ and ∼45 nm for $La_{0.63}Sr_{0.37}MnO_3$. Both systems with selected strontium concentrations close to optimal doping level $x \sim 0.33$ were chosen in order to neglect an extra

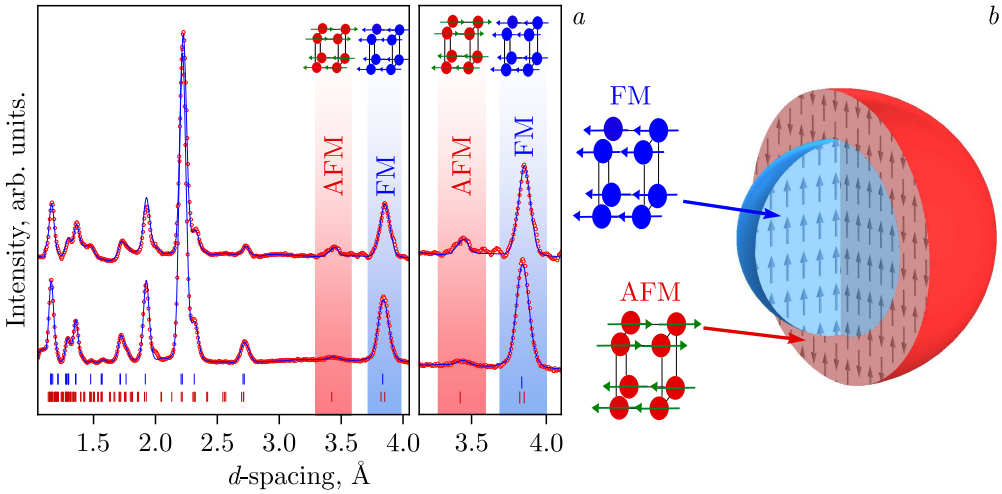

Figure 1. *a*) Neutron diffraction patterns and zoomed parts of the magnetic peaks of the nanostructured manganites $La_{0.72}Sr_{0.28}MnO_3$ and $La_{0.63}Sr_{0.37}MnO_3$, measured at ambient pressure and at low temperature. Observed magnetic peaks correspond to ferromagnetic (FM) and antiferromagnetic (AFM) phases that are labeled in blue and red, respectively. *b*) The schematic of magnetic phase separation in manganite nanoparticles. The blue area depicts the FM component in the core of nanoparticle. The AFM phase is represented in red. The figures represent adapted data from the previous papers [81, 82].

effect from possible strontium content fluctuations. The neutron diffraction patterns of $La_{0.63}Sr_{0.37}MnO_3$ and $La_{0.72}Sr_{0.28}MnO_3$ measured at ambient pressure and low temperature are shown in Figure 1. Over the whole studied temperature range of 10–300 K, both the nanostructured manganites retain the average rhombohedral structure of the $R\bar{3}c$ symmetry. The increasing intensity of the diffraction peaks at $d_{hkl} \sim 3.8$ Å and ~ 2.7 Å on cooling evidences development of the FM order in both nanostructured manganites (Figure 1, *a*). The values of the ordered Mn magnetic moments estimated from the Rietveld refinement of the diffraction data at $T = 4$ K are $M_{FM} = 2.3(4)\ \mu_B$ for $La_{0.63}Sr_{0.37}MnO_3$ and $M_{FM} = 2.2(2)\ \mu_B$ for $La_{0.72}Sr_{0.28}MnO_3$ samples, respectively [81]. It should be highlighted that these values are significantly smaller than the theoretical value of $\sim 3.7\ \mu_B$ per Mn for the ideal FM alignment, as observed for bulk materials [93]. Based on the results of this neutron experiment, we can assume that the manganese oxide nanoparticles show a slight excess of oxygen that can primarily be attributed to the surface area [81, 82]. We proposed that this effect is related to occurrence of the magnetically inactive layer (or "magnetically dead" shell) on manganite nanoparticles [81]. It also contributes to the surface strain that compresses the particle core and alters its physical properties. Recently, it has been discovered that ultrafine magnetite Fe_3O_4 nanoparticles with a well-defined crystal structure extending to the outermost layers and a surface that is shielded from excessive oxidation do not necessarily show a reduction in the ordered magnetic moment [94]. The calculated "magnetically dead layer" is about 1.5 nm thick in both $La_{1-x}Sr_xMnO_3$ nanoparticles [82]. Therefore, the surface quality of the nanoparticles is a reasonable origin for observed modification of magnetic properties in the nanostructured manganites under study.

When cooling the both samples, a weak extra magnetic peak was observed at $d_{hkl} \sim 3.5$ Å (Figure 1). Based on the analysis of the obtained neutron diffraction data, this property is attributed to production of the A-type AFM ordering coexisting with the FM one [95]. The fractions of FM and AFM phases were estimated from neutron diffraction data using Rietveld refinement, based on the analysis of the magnetic reflections particular of each magnetic or-

dering. The ordered Mn magnetic moments in this AFM structure are aligned within the (*ac*) crystallographic planes, while in adjacent planes along the *b*-axis they are oriented in the opposite direction. It should be highlighted that the position of the AFM peak is estimated in the framework of a simplified cubic perovskite structure with an average lattice parameter of $\langle a_p \rangle = 3.85$ Å [81]. Nevertheless, the parameters of the rhombohedral structure of this manganite are based on the perovskite lattice with a lattice parameter of $\langle a_p \rangle = 3.82$ Å [96]. To obtain the Curie temperature T_C for the ferromagnetic phase and the Néel temperature T_N for the antiferromagnetic phase, the $M(T)$ data corresponded to the function [97, 98]:

$$\frac{M}{M_0} = B_S\left(\frac{3S}{S+1}\frac{M}{M_0}\frac{T_C}{T}\right), \tag{1}$$

where B_S is the Brillouin function, S is the spin of the system ($S = 3/2$), and M_0 is the magnetic moment at $T = 0$. The Curie temperatures T_C for the ferromagnetic phase were calculated as 308(1) and 304(1) K and the Néel temperatures T_N were estimated almost equally as 265(1) K for nanostructured $La_{0.72}Sr_{0.28}MnO_3$ and $La_{0.68}Sr_{0.37}MnO_3$ manganites, respectively.

It was assumed that the development of the A-type AFM phase is associated with the anisotropic deformation of the MnO_6 oxygen octahedra [95, 96]. Intriguingly, in the rhombohedral structure of nanostructured manganese oxides, the oxygen octahedra show high symmetry and consist of identical Mn–O bonds [95]. Consequently, the AFM phase in bulk $La_{1-x}Sr_xMnO_3$ manganites was not anticipated. However, for nanostructured manganites, the antiferromagnetic phase has been directly identified using neutron diffraction.

Let us discuss the nature and mechanisms of magnetic phase separation phenomena in nanostructured manganites. We consider the possibility that the non-stoichiometry of oxygen on the surface of manganese nanoparticles might be responsible for the occurrence of an extra structural phase with a lower symmetry than the rhombohedral phase in bulk manganites [81, 82]. In accordance with the structural phase diagram of $La_{1-x}Sr_xMnO_3$ manganites, we can propose a structural model where the initial rhombohedral structure undergoes a transformation into the tetragonal phase with the $I4/mcm$ space group. This tetragonal phase then evolves into the orthorhombic phase with the $Fmmm$ space group that is accompanied by the orbital ordering. In this case, the predominant magnetic state for this distortion structure is an A-type antiferromagnetic one. Consequently, in accordance with our experimental results and recent theoretical models [24], two distinct magnetic phases can coexist and correspond to a structural phase separation that can be conceptualized as an inner ferromagnetic (FM) core based on a rhombohedral framework, surrounded by a shell of the antiferromagnetic phase developed on a distorted orthorhombic lattice (Figure 1, *b*). Development of this complex nanoscale structural arrangement causes strong modification of magnetic properties of nanostructured materials with respect to bulk analogues, observed experimentally.

To validate our proposed core-shell prototype for manganese oxide nanoparticles in future, we subjected the studied nanostructured materials to extra mild acid leaching process [82]. The suppression of the A-type AFM ordering in leached $La_{1-x}Sr_xMnO_{3+\delta}$ nanoparticles occurs due to the stabilization of their bare surface using citrate ions. Citrate anions form a coordinate covalent bond with metal cations like Mn^{3+}/Mn^{4+} and might complete the MnO_6 octahedra on the surface of manganite nanoparticles. We carried out a comparative analysis of as-prepared and mildly acid-leached manganite nanoparticles. As a result, the nanoparticles lost their original AFM component after additional chemical treatment and showed purely FM order. The spontaneous magnetic moments, estimated using linear extrapolation from high-field magnetization at 4.5 K, make 45.2 $A \cdot m^2 \cdot kg^{-1}$ (1.81 μ_B per Mn) and 48.4 $A \cdot m^2 \cdot kg^{-1}$

(1.96 μ_B per Mn) for the as-grown and leached $La_{0.64}Sr_{0.36}MnO_{3+\delta}$ nanoparticles, respectively. In the case of the leached manganese nanoparticles, the A-type antiferromagnetic phase is either nonexistent or negligible.

3.2. Pressure effects on the crystal and magnetic structure of manganite nanoparticles

As we have discussed above, the magnetic phase separation effects revealed in manganite nanoparticles are related to structural phase separation. One may expect that the different lattice symmetry in the core and shell of the nanoparticles may provoke distinct evolution of lattice strain upon compression by application of high pressure and give rise to novel pressure-induced phenomena. In order to prove this assumption, the crystal and magnetic structures of nanostructured manganites $La_{0.63}Sr_{0.37}MnO_3$ and $La_{0.72}Sr_{0.28}MnO_3$ have been studied using the neutron diffraction in the pressure range up to 5 GPa [81, 82].

The pressure dependences of the rhombohedral lattice parameters in the hexagonal setting and unit cell volume of studied nanostructured manganites have been obtained. The linear compressibility coefficients $k_{ai} = -(1/a_{0i})(da_i/dP)\big|_T$ ($a_i = a$ and c) were calculated to be $k_a = 0.01148(7)$ and $k_c = 0.00386(2)$ GPa^{-1} for $La_{0.63}Sr_{0.37}MnO_3$ and $k_a = 0.0121(3)$ and $k_c = 0.0045(4)$ GPa^{-1} for the $La_{0.72}Sr_{0.28}MnO_3$ samples. It can be seen that the compressibility of both systems is anisotropic, with the compressibility coefficient along the trigonal c-axis being three times smaller than that along the perpendicular a-axis.

The unit cell volume compressibility data correspond to the third-order Birch–Murnaghan equation of state [99]:

$$P = \frac{3}{2}B_0(x^{-7/3} - x^{-5/3})\left[1 + \frac{3}{4}(B' - 4)(x^{-2/3} - 1)\right], \quad (2)$$

where $x = V/V_0$ is the relative volume of unit cell and V_0 is the unit cell volume at $P = 0$; B_0 and B' are the bulk modulus $B_0 = -V(dP/dV)_T$ and its pressure derivative $B' = (dB_0/dP)_T$. The best fit is achieved by $B_0 = 127(5)$ GPa and $B' = 4(1)$ for $La_{0.63}Sr_{0.37}MnO_3$ manganite and $B_0 = 156(5)$ GPa and $B' = 4(1)$ for $La_{0.72}Sr_{0.28}MnO_3$ one. Due to the occurrence of disordered surface layer in the nanoparticles, the obtained values are somewhat lower in comparison to those for bulk samples [96, 100, 101].

At high pressure, the intensity of antiferromagnetic peaks in neutron diffraction patterns increases, while the relevant contribution to nuclear peaks from the FM phase is suppressed (Figure 2, *a*). In the pressure range 0–4.5 GPa, the ordered Mn magnetic moment of the FM state at $T = 5$ K decreases from 2.3(3) to 1.4(4) μ_B and from 2.2(2) to 1.3(4) μ_B for $La_{0.63}Sr_{0.37}MnO_3$ and $La_{0.72}Sr_{0.28}MnO_3$, respectively. At the same time, the ordered Mn magnetic moments of the A-type AFM component increase from 1.6(2) to 2.9(2) μ_B and from 0.3(3) to 2.3(5) μ_B for $La_{0.63}Sr_{0.37}MnO_3$ and $La_{0.72}Sr_{0.28}MnO_3$ nanoparticles, respectively [80]. These observations can be interpreted as an increase in the fraction of the A-type AFM phase, accompanied by a corresponding decrease in the fraction of the FM phase. In a preliminary analysis, where the FM and AFM phases are aligned to a comparable degree and contain equal quantities of the "dead" non-magnetic surface layer, we calculate the proportion of the ferromagnetic and antiferromagnetic phases in nanostructured manganites (Figure 2, *b*). At ambient pressure, the FM and AFM magnetic phase fractions were obtained as 59% : 41% for $La_{0.63}Sr_{0.37}MnO_3$ and 88% : 12% for $La_{0.72}Sr_{0.28}MnO_3$, respectively. At high pressure, the value of FM:AFM ratio is changed to 32% : 67% for $La_{0.63}Sr_{0.37}MnO_3$ and 36% : 64% for $La_{0.72}Sr_{0.28}MnO_3$.

The temperature dependences of the ordered Mn magnetic moment M for the FM and AFM phases are shown in Figure 2, *d*.

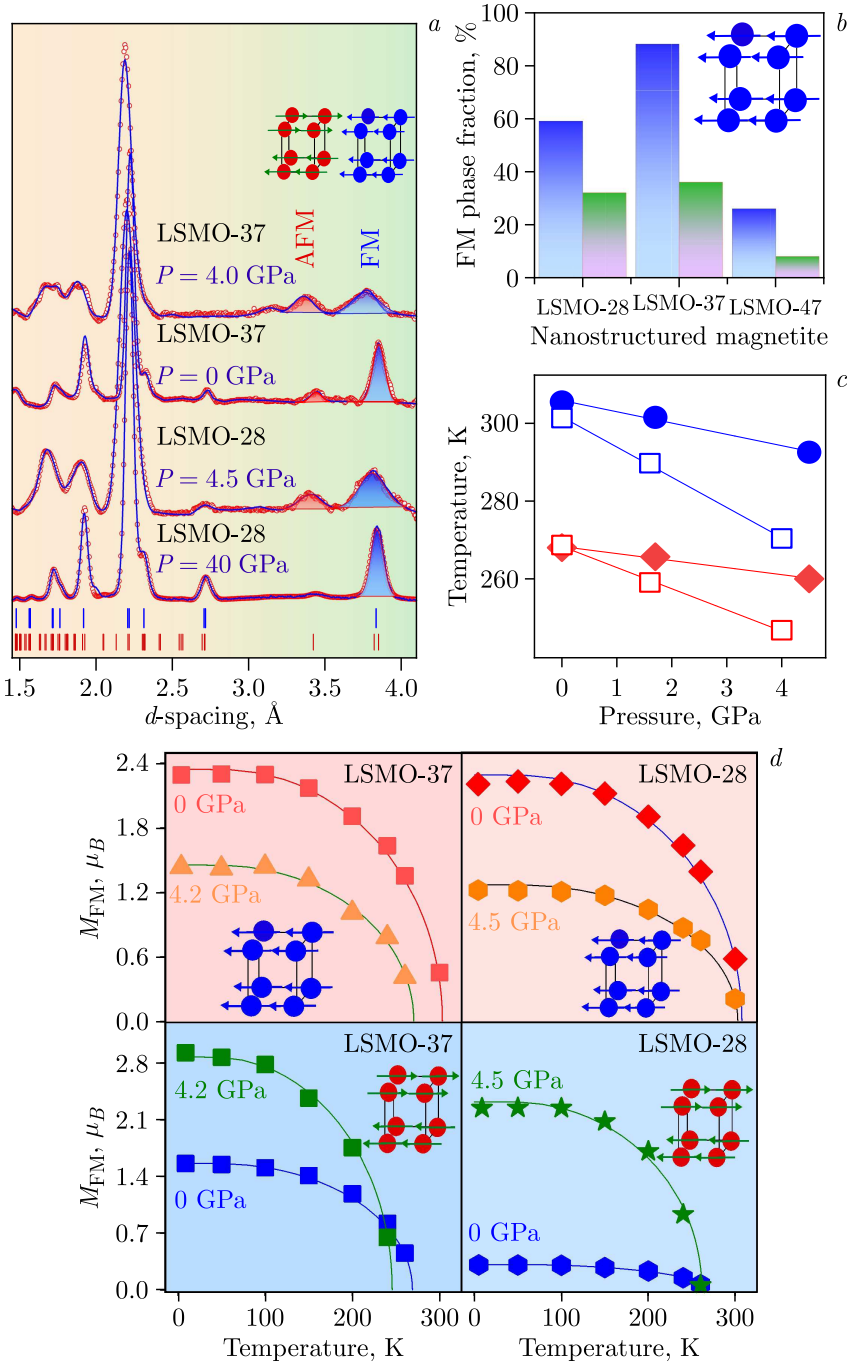

Figure 2. *a*) Neutron diffraction patterns of the nanostructured manganites $La_{0.63}Sr_{0.37}MnO_3$ (LSMO-37) and $La_{0.72}Sr_{0.28}MnO_3$ (LSMO-28), measured at high pressure and low temperature. Experimental points and fitting profiles are shown and the positions of the magnetic peaks of the A-type antiferromagnetic and ferromagnetic components of the magnetic structure are marked as "AFM" and "FM", respectively. *b*) Diagram of the fraction of the FM component in a nanoparticle of manganites $La_{0.63}Sr_{0.37}MnO_3$ (LSMO-37), $La_{0.72}Sr_{0.28}MnO_3$ (LSMO-28) and $La_{0.53}Sr_{0.47}MnO_3$ (LSMO-47) at ambient pressure (blue bars) and at high pressure (green bars). *c*) Curie (blue symbols) and Néel (red symbols) temperatures of $La_{0.72}Sr_{0.28}MnO_3$ (open symbols) and $La_{0.63}Sr_{0.37}MnO_3$ (close symbols) as a function of pressure. The solid lines represent linear fits to the experimental data. *d*) The temperature dependences of the Mn magnetic moment of the FM and AFM phases of nanostructured manganites. The experimental data corresponded to the function (1).

Besides, the applied pressure results in a decrease in both the Curie temperature T_C and the Néel temperature T_N for nanostructured manganites [82, 83]. The obtained values of T_C and T_N as functions of pressure are shown in Figure 2, *c*. The Curie temperatures decrease almost linearly with coefficients $dT_C/dP = -8.2(3)$ and $-2.1(1)$ K · GPa^{-1} for $La_{0.63}Sr_{0.37}MnO_3$ and $La_{0.72}Sr_{0.28}MnO_3$, respectively. The Néel temperatures of transition to the antiferromagnetic state decrease with coefficients $dT_N/dP = -5.6(3)$ and $-1.9(1)$ K · GPa^{-1} for $La_{0.63}Sr_{0.37}MnO_3$ and $La_{0.72}Sr_{0.28}MnO_3$, respectively. The unexpected decreasing in the Curie temperature of transition to the ferromagnetic state contradicts the results obtained for bulk rhombohedral manganites within the double exchange model [15, 96]. The Curie temperatures for the half-doped nanostructured (200-nm nanoparticles) compound $La_{0.53}Sr_{0.47}MnO_3$ are found to decrease significantly with rather large pressure coefficient $dT_C/dP = -8.1(2)$ K · GPa^{-1}. It is interesting to state that for the bulk manganites, the Curie temperature generally increases at high pressure (for instance, $dT_C/dP = 4.3$ GPa^{-1} for the rhombohedral $La_{0.7}Sr_{0.3}MnO_3$ [96]). The Néel temperatures of the A-type AFM phase for nanostructured manganite $La_{0.53}Sr_{0.47}MnO_3$ slightly increase with $dT_N/dP = 0.6(3)$ K · GPa^{-1}. We can calculate the average proportions of the ferromagnetic and antiferromagnetic phases in the nanostructured manganite $La_{0.53}Sr_{0.47}MnO_3$ at a pressure of 2.1 GPa to be 26% and 74%, respectively. At higher pressure of 5.5 GPa, the proportion of the magnetic phases FM:AFM in this material is shifted to 8% : 92%, respectively. Therefore, it can be concluded that the application of pressure almost completely changes the predominant magnetic state in the nanostructured manganite $La_{0.53}Sr_{0.47}MnO_3$ from ferromagnetic to antiferromagnetic [15, 83].

A significant change in the proportion of FM and AFM phases can be attributed to the occurrence of pronounced lattice strains in manganese oxide nanoparticles [102–104]. These strains are associated with structural deformations on the manganite nanoparticle surface that can be controlled by the synthesis process. These types of strains may result in changes in the magnetic structure of nanoparticles less than 40 nm or in thin films of manganites [102]. The strains induced by pressure are detected through the pronounced anisotropy of the compression of unit cell parameters and the lengths of Mn–O bonds compared to bulk manganite compounds. The majority of the strain is focused near the surface of the nanoparticles and gradually decreases towards the centre of the particle. These areas have a negligible impact on the overall properties of manganites in the bulk form, but they are crucial for the behavior of magnetic nanoparticles.

3.3. Properties of the crystal and magnetic structure of ferrite nanoparticles

In ferrite nanoparticles, as in nanostructured manganites, there is a strong dependence of magnetic properties on structural defects in the crystal structure [84–86]. The binary oxide $Zn_xFe_{3-x}O_4$, as a model nanostructured ferrite material, belongs to the family of ferrites with a magnetite-type spinel structure, and it is characterized by ferrimagnetic or canted spin ordering with a strong dependence on oxygen stoichiometry and the cation distribution between the two crystallographic sites [83, 84]. Neutron diffraction allows us to investigate the crystal structure in detail, including the redistribution of ions and its impact on the magnetic structure of these systems. We studied the crystal and magnetic structure of zinc-doped ferrite $Zn_{0.34}Fe_{2.53}O_4$ in the form of spherical nanoparticles [84] with an average size of 14 nm (Figure 3, *a*). This compound has the spinel-type crystal structure of $Fd\bar{3}m$ symmetry (Figure 3, *b*), in which the Fe atoms are distributed between the A sites with tetrahedral oxygen coordination and the B sites with octahedral oxygen coordination.

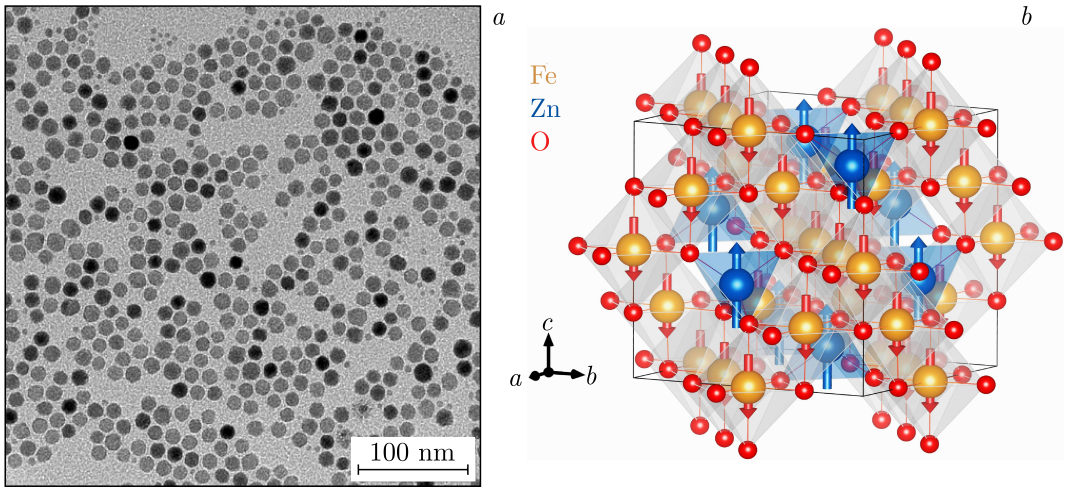

Figure 3. *a*) Transmission electron micrograph of the studied $Zn_{0.34}Fe_{2.53}\square_{0.13}O_4$ nanoparticles; *b*) crystal structures and the magnetic structure of nanostructured ferrite. The figures represent adapted data from the previous paper [84].

In well-crystallized bulk spinels, the structural formula can be $(Zn^{2+}_{2+x}Fe^{3+}_{1-x})[Fe^{2+}/^{3+}]_2O_4$, where round and square brackets indicate tetrahedral (A) and octahedral [B] sites, respectively. This cation distribution reflects the strong preference of Zn^{2+} for A sites and the tendency of $Fe^{2+}/^{3+}$ ions to occupy B sites, consistent with the inverse spinel arrangement. In contrast, the synthesis of nanocrystalline forms, often involving specific thermal or mechanical treatments, frequently results in a partial disorder of Zn and Fe ions between the tetrahedral and octahedral sites. Additionally, the large surface-to-volume ratio of nanoparticles can promote partial oxidation of Fe^{2+} to Fe^{3+}, resulting in non-stoichiometric compounds resembling maghemite.

Our neutron diffraction data provided detailed information on lattice parameters, interatomic bond lengths and angles, as well as the ordered magnetic moments of iron ions at different crystallographic sites in a spinel structure. Furthermore, Mössbauer spectroscopy was used to estimate the Fe^{3+}/Fe^{2+} ratio, as well as the distribution of Zn and Fe ions between the tetrahedral (A) and octahedral [B] sites. The resulting cation arrangement indicates the occurrence of cation vacancies at the B sites, denoted by the symbol $\square$, which quantify the non-stoichiometry arising from partial oxidation of the ferrite. The distribution of Zn and Fe ions between the A and B sites is estimated as $(Fe^{3+}_{0.82}Zn^{2+}_{0.18})_A[Fe^{3+}_{1.44}Fe^{2+}_{0.27}Zn^{2+}_{0.16}\square_{0.13}]_BO_4$, where the B-site vacancy $\square$ quantifies the cation non-stoichiometry due to partial oxidation of the ferrite [84].

By increasing the temperature from 10 to 300 K, the Fe_A–O and Fe_B–O bond lengths, related to A and the B cation sites with tetrahedral and octahedral oxygen coordination, increase linearly. The calculated linear expansion coefficients $\left(k_{Fe-O} = \left(\frac{1}{l_{Fe-O}}\right)\left(\frac{dl_{Fe-O}}{dT}\right)\Big|_{P=0\ GPa}\right)$ for Fe_A–O and Fe_B–O bond lengths at ambient pressure are $k_{FeA-O} = 0.566(3)\cdot10^{-4}$ and $k_{FeB-O} = 0.328(2)\cdot10^{-4}$ K^{-1}, respectively. The predominance of vacancies in the octahedral sites in the studied $Zn_{0.34}Fe_{2.53}\square_{0.13}O_4$ ferrite nanoparticles is the key factor that explains the disparity in the thermal expansion coefficients of the nanostructured and bulk ferrite spinels.

The magnetic moments of Fe ions in different sites are ordered in antiparallel (Figure 3, *b*). Based on the analysis of neutron diffraction data, the relevant ordered magnetic moment values were calculated as $M_A = 3.1(4)$ μ_B for the A sites and $M_B = 3.9(4)$ μ_B for the B sites at 5 K. At room temperature, a minor decrease of intensities of the diffraction peak (111) at

$d_{hkl} \approx 4.82$ Å was observed. The slight decrease in magnetic moments can be attributed to the high Curie temperature of the $Zn_{0.34}Fe_{2.53}\square_{0.13}O_4$ ferrite. In fact, the Curie temperature T_C of relevant nanostructured $Zn_{0.36}Fe_{2.64}O_4$ is above 420 K and according to some references, the Curie temperature has been observed as an anomaly in the DC susceptibility curve at $T_C \approx 700$ K.

Another interesting system for analysis of the physical properties of nanostructured ferrite materials includes the $CoFe_2O_4$ nanoparticles produced during grinding [104]. The $CoFe_2O_4$ ferrite refers to a type of inverse spinel structure, where Co^{3+} ions occupy both tetrahedral and octahedral sites in the cubic crystal lattice. The relative cation distribution between two non-equivalent crystallographic sites may depend on various factors, such as the synthesis conditions, nanoparticle size, vacancies and changes in the magnetic properties of the $CoFe_2O_4$ ferrite. We have previously carried out a systematic investigation of the structural and magnetic properties of $CoFe_2O_4$ nanoparticles with a cubic spinel crystal structure. The average crystal size D ranges from 334 nm for the initial bulk material to about 12 nm after 120 min of grinding. Our results show that the process of high-energy grinding results in the migration of Co^{2+} ions from the octahedral B site to the tetrahedral A site. The grinding driven changes in cation distribution enhance the saturation magnetization and provoke canted magnetic ordering in the $CoFe_2O_4$ nanoparticles [104]. These effects are caused by surface structural disordering.

3.4. Pressure effects on the crystal and magnetic structure of ferrite nanoparticles

First, it should be emphasized that high pressure effects on the crystal, magnetic structure and physical properties of various bulk ferrite materials, in particular, the parent magnetite Fe_3O_4, have been extensively explored. At pressures about 25 GPa, this compound undergoes a phase transition from the cubic spinel $Fd\bar{3}m$ structure to the orthorhombic post-spinel structure of $Bbmm$ symmetry [105]. Additionally, a crossover from a high-spin state to a low-spin state of Fe^{3+} ions has been observed at pressures around 40 GPa [106].

In contrast to bulk Fe_3O_4, the high-pressure behavior of nanostructured ferrites is less explored. In this case, the occurrence of the vacancy defects within the crystal structure of nanoparticles can modify the physical properties significantly. We have studied the structural properties of cation deficient nanostructured zinc ferrite $Zn_{0.34}Fe_{2.53}\square_{0.13}O_4$ using X-ray diffraction and Raman spectroscopy at high pressures up to 34 GPa [86]. The XRD patterns of $Zn_{0.34}Fe_{2.53}\square_{0.13}O_4$ nanoparticles measured at selected pressures and room temperature are shown in Figure 4, *a*. At pressures exceeding 18 GPa, notable changes in the X-ray diffraction data were detected, showing the structural phase transition that occurred. The analysis using the Rietveld method has shown that the observed changes in the XRD data correspond to the occurrence of the post-spinel phase with $Bbmm$ space group (Figure 4, *b*) of the orthorhombic $CaTi_2O_4$ structural type [105, 107]. The phase transition evolves in a gradual way with the $Fd\bar{3}m$ and $Bbmm$ phases coexistence over a wide pressure range. At 18 GPa, a relatively small fraction of the orthorhombic phase of 12% was detected. At a maximum pressure of 32 GPa in our experiments, a fraction of 43% of this phase has been reached. A similar two-phase coexistence was also observed during the pressure-induced phase transition in bulk zinc ferrites. We believe this effect is caused by significant impact of grain size on internal strains and stresses in materials at high pressures.

The pressure evolution of the lattice parameters and the unit cell volume of $Zn_{0.34}Fe_{2.53}\square_{0.13}O_4$ are shown in Figure 4, *c*. In particular, the calculated value of the bulk modulus for the cubic phase of $Zn_{0.34}Fe_{2.53}\square_{0.13}O_4$ ferrite is $B_0 = 185(2)$ GPa. This value is

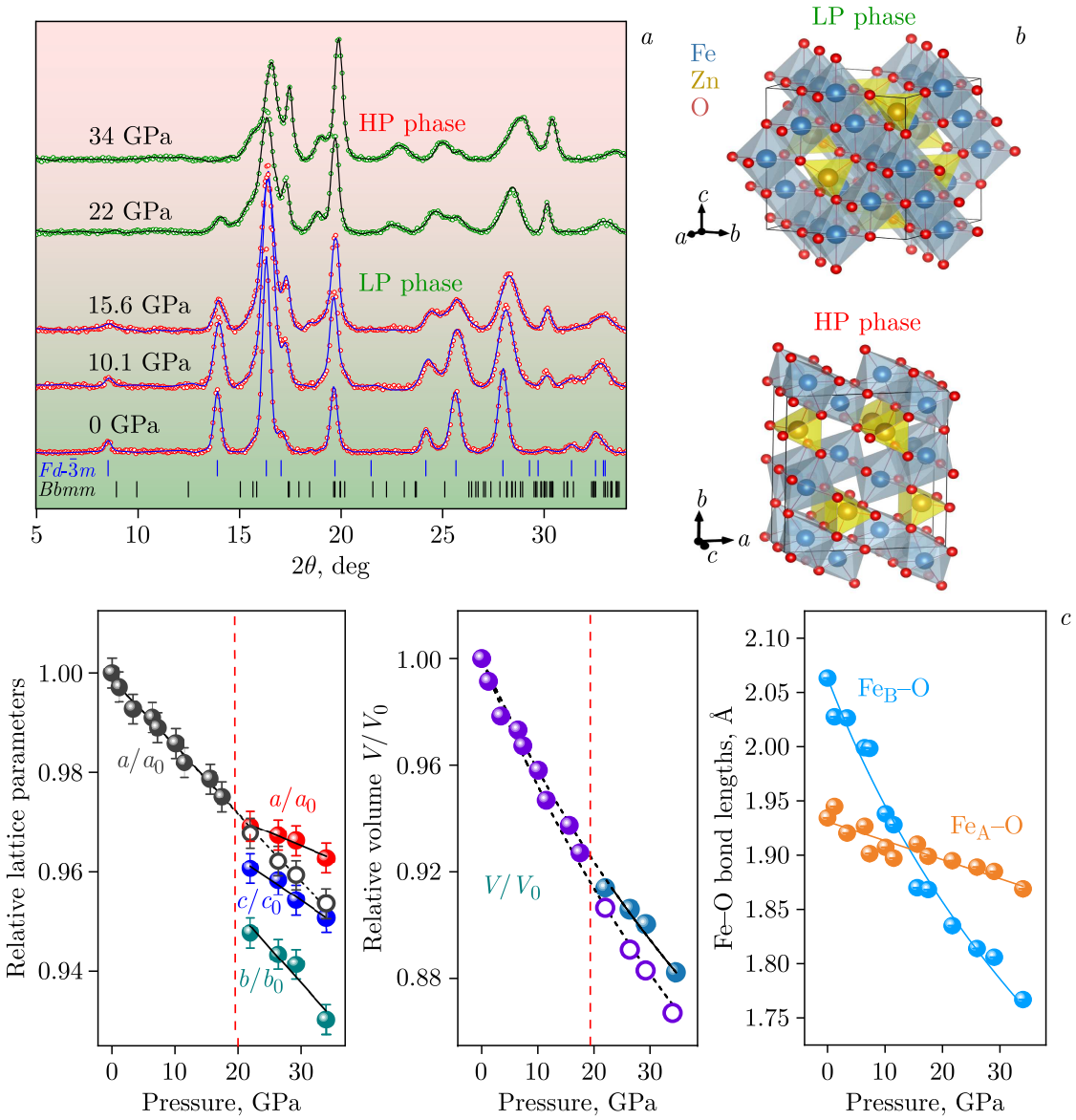

Figure 4. *a*) X-ray diffraction patterns of the nanostructured spinel ferrite $Zn_{0.34}Fe_{2.53}\square_{0.13}O_4$ measured at selected pressures and room temperature. *b*) The schematic of crystal structures for low pressure cubic (LP phase) and pressure-induced orthorhombic (HP) phases of $Zn_{0.34}Fe_{2.53}\square_{0.13}O_4$ ferrite; *c*) the pressure dependences of the unit cell parameters, unit cell volume and Fe–O bond lengths of cubic and pressure-induced orthorhombic phases of the nanostructured $Zn_{0.34}Fe_{2.53}\square_{0.13}O_4$ ferrite. The open symbols correspond to the data for the cubic phase for pressures above 20 GPa. The figures represent adapted data from the previous paper [86].

comparable to those previously obtained for related spinel-type compounds: $B_0 \sim 186(2)$ GPa for nanostructured $ZnFe_2O_4$; $B_0 \sim 196(2)$ GPa for $CaFe_2O_4$ [106, 107], and $B_0 \sim 188(3)$ GPa for $MgFe_2O_4$ [108, 109].

For nanostructured $Zn_{0.34}Fe_{2.53}\square_{0.13}O_4$ ferrite, the Fe_B-O bonds related to the B cation sites show more pronounced pressure-induced contraction (Figure 4, *c*) with a pressure coefficient ($k_{Fe-O} = -(1/l_{Fe-O})(dl_{Fe-O}/dP)_T$) of $k_{FeB-O} = 4.95(1)\cdot10^{-3}$ GPa^{-1}. The Fe_A–O bonds related to the A cation sites are less affected with a corresponding coefficient of $k_{FeA-O} = 1.06(3) \times 10^{-3}$ GPa^{-1}. We assume that this difference is primarily due to a significant number of vacancies available on the octahedral B site. Additional Raman spectroscopy experiments at high pressure

confirm this assumption. Upon increasing pressure above 18 GPa, a clear splitting of the A_{1g} band has been observed [86].

The high pressure effects on the crystal structure of $CoFe_2O_4$ ferrite were studied using X-ray diffraction (Figure 5, *a*). The Rietveld analysis has shown that phase transition to the post-spinel orthorhombic phase, occurring around 20 GPa, has a gradual character and it evolves over a wide pressure range, in which two phases coexist (Figure 5, *b*). The evolution of the pressure-induced phase is accompanied by a gradual suppression of the ordered Fe magnetic moments [87]. The lattice compression of the orthorhombic phase is found anisotropic with a similar pressure behavior of the *a* and *b* parameters and less pronounced compressibility of the lattice parameter *c* [87]. Such an anisotropy in the compression of the lattice parameters of the post-spinel orthorhombic phase indicates the distortion of Fe–O polyhedra (Figure 5, *c*), arising from Jahn–Teller deformation around divalent and trivalent cobalt and iron ions [87]. The lowering of the symmetry of the crystal structure that provokes compression anisotropy and more pronounced distortion of oxygen polyhedra in the pressure-induced orthorhombic phase plays a significant role in magnetic moment collapse and suppression of initial ferrimagnetic order.

The magnetic interactions in the spinel cubic phase of $CoFe_2O_4$ ferrite are mediated through a complex interplay of superexchange interactions, where the interatomic distances and angles play an important role. Our results show that $Fe(Co)_A$–O–$Fe(Co)_B$ angle decreases slightly from 124.5(5)° to 123.5(5)° under compression up to 23 GPa. The angle values $Fe(Co)_A$–O–$Fe(Co)_A$ of 92.1(5)° and $Fe(Co)_B$–O–$Fe(Co)_B$ of 88.2(5)° obtained at ambient pressure do not show

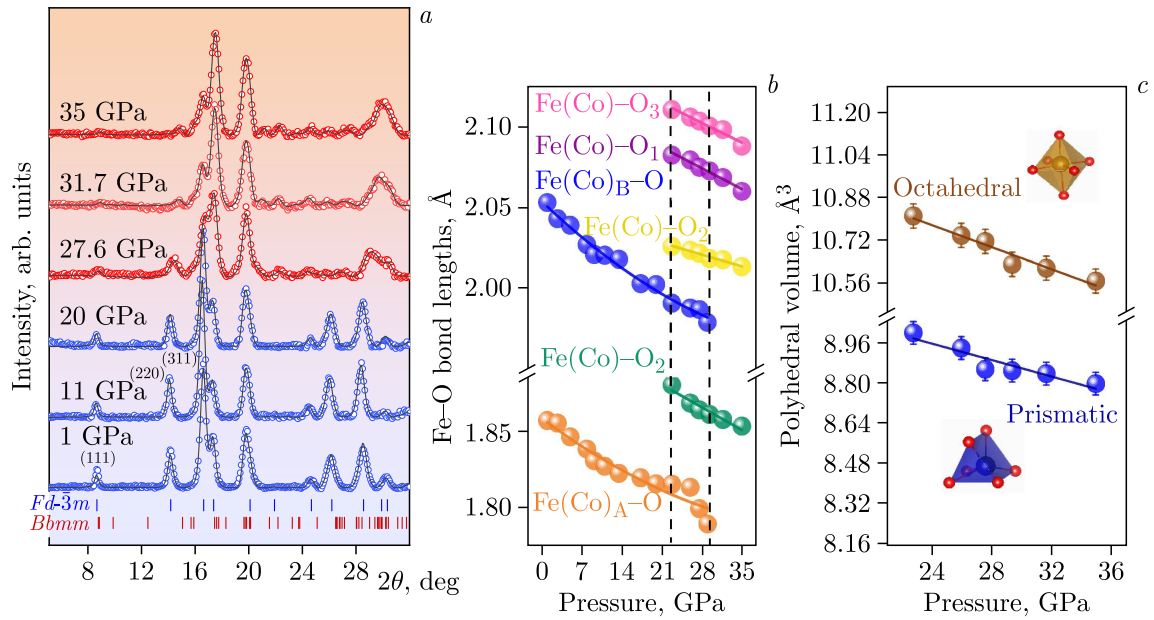

Figure 5. *a*) X-ray diffraction patterns of $CoFe_2O_4$ obtained at selected pressures and at a room temperature and refined using the Rietveld method. Experimental points and calculated profiles are presented. The ticks represent the calculated positions of diffraction peaks for the cubic ($Fd\bar{3}m$ space group) and pressure-induced orthorhombic phases (*Bbmm* space group). *b*) The pressure dependences of the Fe–O bond lengths in $CoFe_2O_4$ ferrite and the volumes of the octahedral and prismatic structural units of $CoFe_2O_4$ ferrite for the orthorhombic pressure-induced phase of $CoFe_2O_4$. The solid lines represent a linear fit to the experimental data. The figures represent adapted data from the previous paper [87].

any significant evolution. It means that the relative arrangement of units with tetrahedral and octahedral coordination of oxygen is almost constant. In the orthorhombic phase, the interatomic angles are constrained by symmetry, but there is another important parameter associated with the static cooperative Jahn–Teller distortion of the Fe(Co)O_6 octahedra. It can be characterized by the distortion coefficient using [110, 111]

$$\delta = \left(\frac{1}{3} \sum_i (l_{\mathrm{Fe(Co)-O}_i i} - \langle l_{\mathrm{Fe(Co)-O}} \rangle)^2 \right)^{1/2}, \quad (3)$$

where the summation is taken over three distinct types of Fe(Co)–O bonds and $\langle l_{\mathrm{Fe(Co)-O}} \rangle$ is the average Fe(Co)–O bond length. The δ coefficient for the cubic phase is zero, and it reaches a value of 0.105 Å at pressure $P = 23$ GPa. When the pressure increases, the δ coefficient reaches 0.002 Å at $P = 35$ GPa. This outcome indicates a reduction in the lattice distortion coefficient that may concern the suppression of magnetic polarons in the initial ferrimagnetic phase of the nanostructured $CoFe_2O_4$ ferrite.

Finally, it is important to state that the $CoFe_2O_4$ nanostructured compound shows a significant magnetic anisotropy due to Co^{2+} ions in different crystallographic positions. The change in the oxygen coordination from tetrahedral to prismatic at Fe^{3+} sites under pressure may cause a substantial distortion in the shape of the oxygen polyhedra, resulting in a considerable increase of the quadrupole splitting parameters compared to those of the cubic spinel structure.

4. Conclusions

In our survey, the results of the recent experimental investigations of structural and magnetic properties of nanostructured manganese and iron oxides using neutron diffraction and complementary techniques in a wide range of thermodynamic parameters have been studied. As has been shown, the properties of the structural mechanisms and magnetic states of nanostructured materials are notably different as compared to those of the bulk forms due to the occurrence of surface defects and vacancies.

In the magnetic nanoparticles of the best doped manganites $La_{1-x}Sr_xMnO_3$ ($x = 0.28$ and 0.37) the development of complex magnetic structures involving ferromagnetic core and antiferromagnetic shell has been observed, characterized by a different crystal structure symmetry. Application of high pressure allows adjusting a proportion of the FM and AFM components, resulting in a significant increase of the AFM one. A similar trend was also found for relevant nearly half-doped material $La_{0.53}Sr_{0.47}MnO_3$.

In the $Zn_{0.34}Fe_{2.53}O_4$ ferrite nanoparticles, a distribution of Zn and Fe atoms was precisely estimated and the oxygen vacancies that occurred in the structure were revealed. Unlike relevant bulk ceramic materials with reduced magnetization due to spin canting, in the studied nanoparticles, the relatively large magnetic moment per formula unit is produced at low temperatures. At high pressures, a gradual structural phase transition from the initial cubic spinel phase to the orthorhombic post-spinel phase occurs. A similar structural phase transition, accompanied by ordered magnetic moments suppression, was also evidenced in $CoFe_2O_4$ ferrite under high pressure.

The obtained results elucidate relationships between variation of structural parameters and modification of magnetic states, and they are relevant for understanding the microscopic mechanisms of development of magnetic and other physical properties of the studied and structurally similar nanostructured complex magnetic oxides.

Acknowledgements

O. N. Lis, A. V. Rutkauskas and A. L. Zhaludkevich acknowledge the support of the joint grants of the Russian Science Foundation, RSF 24-42-10003, and the Belarusian Republican Foundation for Fundamental Research (BRFFR), T23RNFM-023.

Author contributions

D. P. Kozlenko: Supervision, Conceptualization; S. E. Kichanov: Conceptualization, Writing — original draft, Writing — review & editing; N. M. Belozerova: Writing — original draft, Investigation (neutron diffraction); O. N. Lis: Investigation (X-ray diffraction), Formal Analysis; A. V. Rutkauskas: Investigation (X-ray diffraction), Formal Analysis; E. V. Lukin: Investigation (X-ray and neutron diffraction); B. N. Savenko: Investigation (neutron diffraction), Formal Analysis; G. S. Rymski: Investigation (sample synthesis); A. L. Zhaludkevich: Investigation (sample synthesis); Z. Jirák: Investigation (sample synthesis), Formal Analysis; N. T. Dang: Investigation (sample synthesis), Formal Analysis (X-ray diffraction).

Conflicts of interest

The authors declare no conflicts of interest.

References

[1] H. Li, T. Brückel, Synthesis of CMR manganites and ordering phenomena in complex transition metal oxides, RWTH Publications (RWTH Aachen), Germany, 2008.

[2] J. W. Lynn, High temperature superconductivity, Springer Science & Business, Germany, 2012.

[3] E. Dagotto, T. Hotta, A. Moreo, Colossal magnetoresistant materials: The key role of phase separation, Physics Reports 344 (2001) 1–153. doi.org/10.1016/s0370-1573(00)00121-6.

[4] C. N. R. Rao, B. Raveau, Colossal magnetoresistance, charge ordering and related properties of manganese oxides. World Scientific Publishing Co. Pte. Ltd, Singapore, 1998.

[5] M. Baldini, T. Muramatsu, M. Sherafati, H. Mao, L. Malavasi, P. Postorino, S. Satpathy, V. V. Struzhkin, Origin of colossal magnetoresistance in $LaMnO_3$ manganite, Proceedings of the National Academy of Sciences 112 (35) (2015) 10869–10872. doi.org/10.1073/pnas.1424866112.

[6] E. L. Nagaev, Colossal-magnetoresistance materials: Manganites and conventional ferromagnetic semiconductors, Physics Reports 346 (6) (2001) 387–531. doi.org/10.1016/s0370-1573(00)00111-3.

[7] E. O. Wollan, W. C. Koehler, Neutron diffraction study of the magnetic properties of the series of Perovskite-type compounds $[(1-x)\mathrm{La}, x\mathrm{Ca}]\mathrm{MnO}_3$, Physical Review 100 (1955) 545–563. doi.org/10.1103/physrev.100.545.

[8] G. Van Tendeloo, O. I. Lebedev, M. Hervieu, B. Raveau, Structure and microstructure of colossal magnetoresistant materials, Reports on Progress in Physics 67 (2004) 1315–1365. doi.org/10.1088/0034-4885/67/8/r01.

[9] J. Van Den Brink, G. Khaliullin, D. Khomskii, Charge and orbital order in half-doped manganites, Physical Review Letters 83 (1999) 5118–5121. doi.org/10.1103/PhysRevLett.83.5118.

[10] G. J. Snyder, Magnetism and electron transport in magnetoresistive lanthanum calcium manganite, 1997.

[11] I. O. Troyanchuk, M. V. Bushinsky, V. A. Khomchenko, V. V. Sikolenko, C. Ritter, S. Schorr, Spin state crossover and colossal magnetoresistance in barium-doped cobaltites, Journal of Physics and Chemistry of Solids 129 (2019) 86–91. doi.org/10.1016/j.jpcs.2018.12.03.

[12] S. B. Krupanidhi, A. Sharma, A. K. Singh, V. Tuli, Recent Advances in Functional Materials and Devices: Select Proceedings of AFMD, Springer Nature, Singapore, 2023.

[13] Roy, R. Gupta, A. Garg, Multiferroic memories, Advances in Condensed Matter Physics 2012 (2012) 1–12. doi.org/10.1155/2012/926290.

[14] N. Boora, R. Ahmad, S. Rahman, N. Q. Dung, A. Ahmad, M. B. Alshammari, B.-I. Lee, Recent advances of colossal magnetoresistance in versatile La–CA–Mn–O material-based films, Magnetochemistry 11 (2025) 1–23. doi.org/10.3390/magnetochemistry11010005.

[15] Yu. A. Izyumov, Yu. N. Skryabin, Double exchange model and the unique properties of the manganites, Physics–Uspekhi 44 (2001) 109–134. doi.org/10.1070/pu2001v044n02abeh000840.

[16] J. M. P. Carmelo, J. M. B. L. D. Santos, V. J. R. Vieira, P. Sacramento, Strongly correlated systems, coherence and entanglement, World Scientific, 2007.

[17] M. B. Salamon, M. Jaime, The physics of manganites: Structure and transport, Reviews of Modern Physics 73 (2001) 583–628. doi.org/10.1103/revmodphys.73.583.

[18] M. C. Martin, G. Shirane, Y. Endoh, K. Hirota, Y. Moritomo, Y. Tokura, Magnetism and structural distortion in the $La_{0.7}Sr_{0.3}MnO_3$ metallic ferromagnet, Physical Review B 53 (1996) 14285. doi.org/10.1103/physrevb.53.14285.

[19] S. JianFei, T. GuangShan, L. TsungHan, Theory of coexistence of charge-ordering and antiferromagnetic phases in $R_{0.5}A_{0.5}MnO_3$, Communications in Theoretical Physics, 33 (3) (2000) 329–334. doi.org/10.1088/0253-6102/33/3/329.

[20] K. Shimazaki, S. Tachikawa, A. Ohnishi, Y. Nagasaka, Temperature dependence of total hemispherical emittance in perovskite-type manganese oxides, $La_{1-x}Sr_xMnO_3$, High Temperatures – High Pressures 33 (2001) 525–531. doi.org/10.1068/htwu129.

[21] D. A. Mota, A. Almeida, V. H. Rodrigues, M. M. R. Costa, P. Tavares, P. Bouvier, M. Guennou, J. Kreisel, J. Moreira Agostinho, Dynamic and structural properties of orthorhombic rare-earth manganites under high pressure, Physical Review B 90 (2014) 054104. doi.org/10.1103/physrevb.90.054104.

[22] D. P. Kozlenko, B. N. Savenko, High-pressure effects on the crystal and magnetic structure of managanites, Physics of Particles and Nuclei 37 (2006) S1–S12. doi.org/10.1134/s106377960607001x.

[23] S. E. Kichanov, D. P. Kozlenko, L. H. Khiem, N. X. Nghia, N. T. T. Lieu, M. T. Vu, E. V. Lukin, D. T. Khan, N. Q. Tuan, B. N. Savenko, N. T. Dang, Magnetic phase transition in $La_{0.8}Sr_{0.2}Mn_{0.9}Sb_{0.1}O_3$ manganite under pressure, Chemical Physics 528 (2020) 110541. doi.org/10.1016/j.chemphys.2019.110541.

[24] D. P. Kozlenko, N. T. Dang, S. E. Kichanov, E. V. Lukin, K. Knizek, Z. Jirák, L. S. Dubrovinsky, V. I. Voronin, B. N. Savenko, Pressure-induced structural transformations, orbital order and antiferromagnetism in $La_{0.75}Ca_{0.25}MnO_3$, The European Physical Journal B 86 (2013) 360. doi.org/10.1140/epjb/e2013-40438-y.

[25] D. P. Kozlenko, E. V. Lukin, S. E. Kichanov, Z. Jirák, N. O. Golosova, B. N. Savenko, High-pressure evolution of the magnetic order in $LaMnO_3$, Physical Review B 107 (2023) 144426. doi.org/10.1103/physrevb.107.144426.

[26] Y. Mita, D. Izaki, M. Kobayashi, S. Endo, Pressure-induced metallization of MnO, Physical Review B 71 (2005) 100101. doi.org/10.1103/physrevb.71.100101.

[27] T. S. Santos, B. J. Kirby, S. Kumar, S. J. May, J. A. Borchers, B. B. Maranville, J. Zarestky, S. G. E. te Velthuis, J. van den Brink, A. Bhattacharya, Delta doping of ferromagnetism in antiferromagnetic manganite superlattices, Physical Review Letters 107 (2011) 167202. doi.org/10.1103/physrevlett.107.167202.

[28] P. Dey, T. K. Nath, Effect of grain size modulation on the magneto- and electronic-transport properties of $La_{0.7}Ca_{0.3}MnO_3$ nanoparticles: The role of spin-polarized tunneling at the enhanced grain surface, Physical Review B 73 (2006) 214425. doi.org/10.1103/physrevb.73.214425.

[29] G. Lehmann, G. Muscas, M. Ferretti, E. Pusceddu, D. Peddis, F. Congiu, Structural and magnetic properties of nanosized half-doped rare-earth $Ho_{0.5}Ca_{0.5}MnO_3$ manganite, Applied Sciences 12 (2022) 695. doi.org/10.3390/app12020695.

[30] E. Natividad, M. Castro, G. Goglio, I. Andreu, R. Epherre, E. Duguet, A. Mediano, New insights into the heating mechanisms and self-regulating abilities of manganite perovskite nanoparticles suitable for magnetic fluid hyperthermia, Nanoscale 4 (2012) 3954–1962. doi.org/10.1039/c2nr30667k.

[31] T. Iwasaki, R. Nakatsuka, K. Murase, H. Takata, H. Nakamura, S. Watano, Simple and rapid synthesis of magnetite/hydroxyapatite composites for hyperthermia treatments via a mechanochemical route, International Journal of Molecular Sciences 14 (2013) 9365–9378. doi.org/10.3390/ijms14059365.

[32] P. G. Radaelli, R. M. Ibberson, D. N. Argyriou, H. Casalta, K. H. Andersen, S. W. Cheong, J. F. Mitchell, Mesoscopic and microscopic phase segregation in manganese perovskites, Physical Review B 63 (2001) 172419. doi.org/10.1103/physrevb.63.172419.

[33] E. Dagotto, J. Burgy, A. Moreo, Nanoscale phase separation in colossal magnetoresistance materials: Lessons for the cuprates?, Solid State Communications 126 (2003) 9–22. doi.org/10.1016/s0038-1098(02)00662-2.

[34] R. D. Sánchez, J. Rivas, C. Vázquez-Vázquez, A. López-Quintela, M. T. Causa, M. Tovar, S. Oseroff, Giant magnetoresistance in fine particle of $La_{0.67}Ca_{0.33}MnO_3$ synthesized at low temperatures, Applied Physics Letters 68 (1996) 134–136. doi.org/10.1063/1.116780.

[35] D. Souza, J. Sahoo, M. Vagadia, S. Rayaprol, L. D. Mendonca, M. D. Daivajna, Particle size-dependent structural and magnetic properties of $Pr_{0.6-x}Bi_xSr_{0.4}MnO_3$ (x = 0.10 and 0.25), Journal of Materials Science: Materials in Electronics 34 (2023) 1901. doi.org/10.1007/s10854-023-11265-1.

[36] H. Dulli, E. W. Plummer, P. A. Dowben, J. Choi, S.-H. Liou, Surface electronic phase transition in colossal magnetoresistive manganese perovskites: $La_{0.65}Sr_{0.35}MnO_3$, Applied Physics Letters 77 (2000) 570–572. doi.org/10.1063/1.127047.

[37] A. Rostamnejadi, H. Salamati, P. Kameli, H. Ahmadvand, Superparamagnetic behavior of $La_{0.67}Sr_{0.33}MnO$ nanoparticles prepared via sol–gel method, Journal of Magnetism and Magnetic Materials 321 (2009) 3126–3131. doi.org/10.1016/j.jmmm.2009.05.035.

[38] M. S. Chavali, M. P. Nikolova, Metal oxide nanoparticles and their applications in nanotechnology, SN Applied Sciences 1 (2019) 607. doi.org/10.1007/s42452-019-0592-3.

[39] K. K. Kefeni, T. A. M. Msagati, B. B. Mamba, Ferrite nanoparticles: Synthesis, characterisation and applications in electronic device, Materials Science and Engineering B 215 (2017) 37–55. doi.org/10.1016/j.mseb.2016.11.002.

[40] D. P. Kozlenko, L. S. Dubrovinsky, S. E. Kichanov, E. V. Lukin, V. Cerantola, A. I. Chumakov, B. N. Savenko, Magnetic and electronic properties of magnetite across the high pressure anomaly, Scientific Reports 9 (2019) 4464. doi.org/10.1038/s41598-019-41184-3.

[41] S. S. Ata-Allah, M. Yehia, Transport properties and conduction mechanisms in $CuFe_2O_4$, $Cu_{1-x}Zn_xGa_{0.3}Fe_{1.7}O_4$ compounds, Physica B: Condensed Matter 404 (2009) 2382–2388. doi.org/10.1016/j.physb.2009.04.044.

[42] J. Wu, N. Li, J. Xu, Y. Jiang, Z.-G. Ye, Z. Xie, L. Zheng, Partially inverse spinel $ZnFe_2O_4$ with high saturation magnetization synthesized via a molten salt route, Applied Physics Letters 99 (2011) 202505. doi.org10.1063/1.3662840.

[43] S. S. Ata-Allah, A. Hashhash, Jahn–Teller effect and superparamagnetism in Zn substituted copper-gallate ferrite, Journal of Magnetism and Magnetic Materials 307 (2006) 191–197. doi.org/10.1016/j.jmmm.2006.04.002.

[44] M. A. Hessien, R. M. Khattab, H. E. H. Sadek, H. H. Abo-Almaged, M. A. Taha, Optimizing magnetic, mechanical, and electrical properties of cobalt-substituted zinc chromite spinel via

microwave-hydrothermal synthesis, Journal of Inorganic and Organometallic Polymers and Materials 35 (2025) 5326–5344. doi.org/10.1007/s10904-025-03592-z.

[45] M. A. Willard, Y. Nakamura, D. E. Laughlin, M. E. McHenry, Magnetic properties of ordered and disordered spinel-phase ferrimagnets, Journal of the American Ceramic Society 82 (1999) 3342–3346. doi.org/10.1111/j.1151-2916.1999.tb02249.x.

[46] E. Prince, Crystal and magnetic structure of copper chromite, Acta Crystallographica 10 (1957) 554–556. doi.org/10.1107/s0365110x5700198x.

[47] A. Akbarzadeh, M. Samiei, S. Davaran, Magnetic nanoparticles: Preparation, physical properties, and applications in biomedicine, Nanoscale Research Letters, 7 (2012) 144. doi.org/10.1186/1556-276x-7-144.

[48] H. Igarashi, K. Okazaki, Effects of porosity and grain size on the magnetic properties of NiZn ferrite, Journal of the American Ceramic Society 60 (1977) 51–54. doi.org/10.1111/j.1151-2916.1977.tb16092.x.

[49] C. Liu, A. J. Rondinone, Z. J. Zhang, Synthesis of magnetic spinel ferrite $CoFe_2O_4$ nanoparticles from ferric salt and characterization of the size-dependent superparamagnetic properties, Pure and Applied Chemistry 72 (2000) 37–45. doi.org/10.1351/pac200072010037.

[50] V. G. Harris, Modern microwave ferrites, IEEE Transactions on Magnetics 48 (2011) 1075–104. doi.org/10.1109/tmag.2011.2180732.

[51] A. Thakur, P. Thakur, Applications of spinel nano-ferrites in health, environmental sustainability, and safety. CRC Press, Boca Raton, 2025.

[52] K. O. Abdulwahab, M. M. Khan, J. R. Jennings, Ferrites and ferrite-based composites for energy conversion and storage applications, Critical Reviews in Solid State and Materials Sciences 49 (2023) 807–55. doi.org/10.1080/10408436.2023.2272963.

[53] A. Aslam, M. U. Islam, I. Ali, Awan, M. Irfan, A. Iftikhar, High frequency electrical transport properties of $CoFe_2O_4$ and $Sr_2NiMnFe_{12}O_{22}$ composite ferrites, Ceramics International 40 (2013) 155–62. doi.org/10.1016/j.ceramint.2013.05.116.

[54] Y. Tsay, Y. C. Chiu, C. M. Lei, Hydrothermally synthesized MG-based spinel nanoferrites: Phase formation and study on magnetic features and microwave characteristics, Materials 11 (2018) 2274. doi.org/10.3390/ma11112274.

[55] Q. A. Pankhurst, J. Connolly, S. K. Jones, J. Dobson, Applications of magnetic nanoparticles in biomedicine, Journal of Physics D: Applied Physics 36 (2003) R167. doi.org/10.1088/0022-3727/36/13/201.

[56] Z. Jirak, M. Kacenka, O. Kaman, M. Marysko, N. M. Belozerova, S. E. Kichanov, D. P. Kozpenko, Role of surface on magnetic properties of nanocrystallites, IEEE Transactions on Magnetics 51 (2015) 1–4. doi.org/10.1109/tmag.2015.2433267.

[57] F. Wang, D. Chen, N. Zhang, S. Wang, L. Qin, X. Sun, Y. Huang, Oxygen vacancies induced by zirconium doping in bismuth ferrite nanoparticles for enhanced photocatalytic performance, Journal of Colloid and Interface Science 508 (2017) 237–247. doi.org/10.1016/j.jcis.2017.08.056.

[58] S. Ameer, I. H. Gul, N. Mahmood, M. Mujahid, Semiconductor-to-metallic flipping in a $ZnFe_2O_4$–graphene based smart nano-system: Temperature/microwave magneto-dielectric spectroscopy, Materials Characterization 99 (2014) 254–265. doi.org/10.1016/j.matchar.2014.11.018.

[59] M. Tahir, M. Imran, Z. H. Shah, M. B. Riaz, S. Riaz, S. Naseem, Phase formation and dielectric properties of $MgFe_2O_4$ nanoparticles synthesized by hydrothermal technique. Heliyon 10 (2024) e29553. doi.org/10.1016/j.heliyon.2024.e29553.

[60] E. Greenberg, G. Kh. Rozenberg, W. Xu, R. Arielly, M. P. Pasternak, A. Melchior, G. Garbarino, On the compressibility of ferrite spinels: A high-pressure X-ray diffraction study of MFe_2O_4 (M = Mg, Co, Zn), High Pressure Research 29 (2009) 764–779. doi.org/10.1080/08957950903424424.

[61] E. Greenberg, W. M. Xu, M. Nikolaevsky, E. Bykova, G. Garbarino, K. Glazyrin, D. G. Merkel, L. Dubrovinsky, M. P. Pasternak, G. Kh. Rozenberg, High-pressure magnetic, electronic, and structural properties of MFe_2O_4 (M = Mg, Zn, Fe) ferric spinels, Physical Review B 95 (2017) 195150. doi.org/10.1103/physrevb.95.195150.

[62] S. Ferrari, R. S. Kumar, F. Grinblat, J. C. Aphesteguy, F. D. Saccone, D. Errandonea, In-situ high-pressure X-ray diffraction study of zinc ferrite nanoparticles, Solid State Sciences 59 (2016) 68–72. doi.org/10.1016/j.solidstatesciences.2016.04.006.

[63] T. Yamanaka, A. Uchida, Y. Nakamoto, Structural transition of post-spinel phases $CaMn_2O_4$, $CaFe_2O_4$, and $CaTi_2O_4$ under high pressures up to 80 GPa, American Mineralogist 93 (2008) 1874–1881. doi.org/10.2138/am.2008.2934.

[64] J. Blasco, G. Subías, J. García, C. Popescu, V. Cuartero, High-pressure transformation in the cobalt spinel ferrites, Journal of Solid State Chemistry 223 (2014) 173–177. doi.org/10.1016/j.jssc.2014.09.028.

[65] H. K. Mao, B. Chen, J. Chen, K. Li, J. F Lin, W. Yang, H. Zheng, Recent advances in high-pressure science and technology, Matter and Radiation at Extremes 1 (2016) 59–75. doi.org/10.1016/j.mre.2016.01.005.

[66] M. Guthrie, Future directions in high-pressure neutron diffraction, Journal of Physics: Condensed Matter 27 (2015) 153201. doi.org/10.1088/0953-8984/27/15/153201.

[67] I. Mirebeau, Magnetic neutron diffraction under high pressure, Comptes Rendus Physique 8 (2007) 737–744. doi.org/10.1016/j.crhy.2007.09.020.

[68] S. Klotz, Techniques in high pressure neutron scattering. CRC Press, Boca Raton, 2012.

[69] Yu. A. Izyumov, Magnetic neutron diffraction, 1970th Edition, Springer Science and Business Media, 2012.

[70] D. Cox, Neutron-diffraction determination of magnetic structures, IEEE Transactions on Magnetics 8 (1972) 161–182. doi.org/10.1109/tmag.1972.1067272.

[71] D. P. Kozlenko, S. E. Kichanov, V. I. Voronin, B. N. Savenko, V. P. Glazkov, E. A. Kiseleva, N. V. Proskurnina, Pressure-induced antiferromagnetism in $La_{0.75}Ca_{0.25}MnO_3$ manganite, Journal of Experimental and Theoretical Physics Letters 82 (2005) 447–451. doi.org/10.1134/1.2142875.

[72] M. T. Vu, D. P. Kozlenko, S. E. Kichanov, I. O. Troyanchuk, E. V. Lukin, L. H. Khiem, B. N. Savenko, Pressure-induced antiferromagnetism in the manganite $La_{0.7}Sr_{0.3}Mn_{0.83}Nb_{0.17}O_3$, Journal of Alloys and Compounds 681 (2016) 527–531. doi.org/10.1016/j.jallcom.2016.04.180.

[73] D. P. Kozlenko, N. T. Dang, S. E. Kichanov, E. V. Lukin, K. Knizek, Z. Jirák, L. S. Dubrovinsky, V. I. Voronin, B. N. Savenko, Pressure-induced structural transformations, orbital order and antiferromagnetism in $La_{0.75}Ca_{0.25}MnO_3$, The European Physical Journal B 86 (2013) 360. doi.org/10.1140/epjb/e2013-40438-y.

[74] D. P. Kozlenko, N. T. Dang, S. E. Kichanov, L. T. P. Thao, A. V. Rutkauskas, E. V. Lukin, B. N. Savenko, N. Tran, D. T. Khan, L. V. Truong-Son, L. H. Khiem, B. W. Lee, T. L. Phan, N. L. Phan, N. Truong-Tho, N. N. Hieu, T. A. Tran, M. H. Phan, High pressure enhanced magnetic ordering and magnetostructural coupling in the geometrically frustrated spinel Mn_3O_4, Physical Review B 105 (2022) 094430. doi.org/10.1103/physrevb.105.094430.

[75] V. Shvetsov, Neutron sources at the Frank Laboratory of Neutron Physics of the Joint Institute for Nuclear Research, Quantum Beam Science 1 (2017) 1–9. doi.org/10.3390/qubs1010006.

[76] V. Belushkin, D. P. Kozlenko, A. V. Rogachev, Synchrotron and neutron-scattering methods

for studies of properties of condensed matter: Competition or complementarity?, Journal of Surface Investigation. X-ray, Synchrotron and Neutron Techniques 5 (2011) 828–855. doi.org/10.1134/s1027451011090047.

[77] V. L. Aksenov, A. M. Balagurov, V. P. Glazkov, D. P. Kozlenko, I. V. Naumov, B. N. Savenko, D.V. Sheptyakov, V. A. Somenkov, A. P. Bulkin, V. A. Kudryashev, V. A. Trounov, DN-12 time-of-flight high-pressure neutron spectrometer for investigation of microsamples, Physica B: Condensed Matter 265 (1999) 258–262. doi.org/10.1016/s0921-4526(98)01392-1.

[78] D. P. Kozlenko, S. E. Kichanov, E. V. Lukin, B. N. Savenko, High-pressure neutron diffraction Study of the crystal and magnetic structure of materials at the pulsed reactor IBR-2: Current opportunities and prospects, Crystallography Reports 66 (2021) 303–313. doi.org/10.1134/s1063774521020073.

[79] D. Kozlenko, S. Kichanov, E. Lukin, B. Savenko, The DN-6 neutron diffractometer for high-pressure research at half a megabar scale, Crystals 8 (2018) 331. doi.org/10.3390/cryst8080331.

[80] D. P. Kozlenko, B. N. Savenko, V. P. Glazkov, V. A. Somenkov, Neutron scattering investigations of structure and dynamics of materials under high pressure at IBR-2 pulsed reactor, Neutron News 16 (2005) 13–15. doi.org/10.1080/10448630500454353.

[81] N. M. Belozerova, S. E. Kichanov, Z. Jirák, D. P. Kozlenko, M. Kačenka, O. Kaman, E. V. Lukin, B. N. Savenko, High pressure effects on the crystal and magnetic structure of nanostructured manganites $La_{0.63}Sr_{0.37}MnO_3$ and $La_{0.72}Sr_{0.28}MnO_3$, Journal of Alloys and Compounds 646 (2015) 998–1003. doi.org/10.1016/j.jallcom.2015.06.154.

[82] N. M. Belozerova, S. E. Kichanov, D. P. Kozlenko, O. Kaman, Z. Jirak, Core-shell magnetic structure of $La_{1-x}Sr_xMn_{3+\delta}$ nanocrystallites, IEEE Transactions on Magnetics 53 (2017) 2300905. doi:10.1109/TMAG.2017.2700394.

[83] N. M. Belozerova, S. E. Kichanov, Z. Jirák, D. P. Kozlenko, O. Kaman, E. V. Lukin, B. N. Savenko, The crystal and magnetic structure of nanostructured manganite $La_{0.53}Sr_{0.47}MnO_3$ at high pressure, Materials Chemistry and Physics 262 (2021) 124310. doi.org/10.1016/j.matchemphys.2021.124310.

[84] N. M. Belozerova, S. E. Kichanov, D. P. Kozlenko, O. Kaman, Z. Jirák, E. V. Lukin, B. N. Savenko, Neutron diffraction study of the crystal and magnetic structures of nanostructured $Zn_{0.34}Fe_{2.53}O_4$ ferrite, Journal of Nanoparticle Research 22 (2020) 121. doi.org/10.1007/s11051-020-04852-4.

[85] D. P. Kozlenko, N. M. Belozerova, S. S. Ata-Allah, S. E. Kichanov, M. Yehia, A. Hashhash, E. V. Lukin, B. N. Savenko, Neutron diffraction study of the pressure and temperature dependence of the crystal and magnetic structures of $Zn_{0.3}Cu_{0.7}Fe_{1.5}Ga_{0.5}O_4$ polycrystalline ferrite, Journal of Magnetism and Magnetic Materials 449 (2017) 44–48. doi.org/10.1016/j.jmmm.2017.09.080.

[86] N. M. Belozerova, O. N. Lis, A. V. Rutkauskas, E. V. Lukin, D. P. Kozlenko, Z. Jirák, B. N. Savenko, N. T. Nguyen, A. L. Zhaludkevich, S. E. Kichanov, Pressure-induced phase transition in nanostructured cation-deficient $Zn_{0.34}Fe_{2.53}\square_{0.13}O_4$ ferrite, Physica B: Condensed Matter 690 (2024) 416210. doi.org/10.1016/j.physb.2024.416210.

[87] N. T. Nguyen, O. N. Lis, A. V. Rutkauskas, E. V. Lukin, D. P. Kozlenko, A. L. Zhaludkevich, S. E. Kichanov, N. Truong-Tho, N. T. Dang, Structural and vibrational properties of $CoFe_2O_4$ ferrite at high pressure, Modern Physics Letters B 39 (2024) 2550066. doi.org/10.1142/s0217984925500666.

[88] T. Kmječ, N. T. Nghiem, N. Truong-Tho, D. P. Kozlenko, S. E. Kichanov, A. V. Rutkauskas, V. T. Nguyen, E. A. Korneeva, D. T. Khan, D. T. Huong Giang, T. L. Phan, D. D. Bich, G. S. Rymski, J. Kohout, V. Chlan, N. T. Dang, Revealing crucial factors governing magnetic properties of high-energy ball-milled $CoFe_2O_4$ nanoparticles, Ceramics International 51 (2024) 5168–5180. doi.org/10.1016/j.ceramint.2024.11.491.

[89] J. Rodríguez-Carvajal, Recent advances in magnetic structure determination by neutron powder diffraction, Physica B: Condensed Matter 192 (1993) 55–69. doi.org/10.1016/0921-4526(93)90108-i.

[90] J. Rodríguez-Carvajal, Developments in FULLPROF for magnetic structure determination in superspace, Acta Crystallographica Section A: Foundations and Advances 77 (2021) C176. doi.org/10.1107/s0108767321095064.

[91] H. M. Rietveld, A profile refinement method for nuclear and magnetic structures, Journal of Applied Crystallography 2 (1969) 65–71. doi.org/10.1107/s0021889869006558.

[92] T. Runčevski, C. M. Brown, The Rietveld refinement method: Half of a century anniversary, Crystal Growth & Design 21 (2021) 4821–4822. doi.org/10.1021/acs.cgd.1c00854.

[93] Kačenka, O. Kaman, Z. Jirák, M. Maryško, P. Veverka, M. Veverka, S. Vratislav, The magnetic and neutron diffraction studies of $La_{1-Sr}MnO_3$ nanoparticles prepared via molten salt synthesis, Journal of Solid State Chemistry 221 (2014) 364–372. doi.org/10.1016/j.jssc.2014.10.024.

[94] A. Radoń, M. Kądziołka-Gaweł, D. Łukowiec, P. Gębara, K. Cesarz-Andraczke, A. Kolano-Burian, P. Włodarczyk, M. Polak, R. Babilas, Influence of magnetite nanoparticles shape and spontaneous surface oxidation on the electron transport mechanism, Materials 14 (2021) 5241. doi.org/10.3390/ma14185241.

[95] N. R. Rao, Charge, spin, and orbital ordering in the perovskite manganates, $Ln_{1-x}A_xMnO_3$ (Ln = rare earth, a = Ca or Sr), The Journal of Physical Chemistry B 104 (2000) 5877–5889. doi.org/10.1021/jp0004866.

[96] P. Kozlenko, I. N. Goncharenko, B. N. Savenko, V. I. Voronin, High pressure effects on the crystal and magnetic structure of $La_{0.7}Sr_{0.3}MnO_3$, Journal of Physics: Condensed Matter 16 (2004) 6755–6762. doi.org/10.1088/0953-8984/16/37/011.

[97] B. Beznosov, V. A. Desnenko, E. L. Fertman, C. Ritter, D. D. Khalyavin, Magnetic and neutron diffraction study of $La_{2/3}Ba_{1/3}MnO_3$ perovskite manganite, Physical Review B: Condensed Matter 68 (2003) 054109. doi.org/10.1103/physrevb.68.054109.

[98] S. Arrott, Approximations to brillouin functions for analytic descriptions of ferromagnetism, Journal of Applied Physics 103 (2008) 07C715. doi.org/10.1063/1.2836337.

[99] F. Birch, Equation of state and thermodynamic parameters of NaCl to 300 kbar in the high-temperature domain, Journal of Geophysical Research: Atmospheres 19 (1986) 4949–4954. doi.org/10.1029/jb091ib05p04949.

[100] I. Dhiman, T. Strässle, L. Keller, B. Padmanabhan, A. Das, Pressure effects on the magnetic structure in $La_{0.5}Ca_{0.5-x}Sr_xMnO_3$ ($0.1 \leqslant x \leqslant 0.4$) manganites, Physical Review B 81 (2010) 104424. doi.org/10.1103/physrevb.81.104424.

[101] P. Kozlenko, V. I. Voronin, V. P. Glazkov, I. V. Medvedeva, B. N. Savenko, Magnetic phase transitions in the iron-doped $Pr_{0.7}Ca_{0.3}Mn_{1-y}Fe_yO_3$ manganites at high pressures, Physics of the Solid State 46 (2004) 484–90. doi.org/10.1134/1.1687866.

[102] D. Pesquera, A. Barla, M. Wojcik, E. Jedryka, F. Bondino, E. Magnano, S. Nappini, D. Gutiérrez, G. Radaelli, G. Herranz, F. Sánchez, J. Fontcuberta, Strain-driven orbital and magnetic orders and phase separation in epitaxial half-doped manganite films for tunneling devices, Physical Review Applied 6 (2016) 034004. doi.org/10.1103/physrevapplied.6.034004.

[103] L. Liang, L. Li, H. Wu, X. Zhu, Research progress on electronic phase separation in low-dimensional perovskite manganite nanostructures, Nanoscale Research Letters 9 (2014) 325. doi.org/10.1186/1556-276x-9-325.

[104] T. Kmječ, N. Nghiem, N. Truong-Tho, D. Kozlenko, S. Kichanov, A. Rutkauskas, V. Nguyen, E. Korneeva, D. Khan, D. Giang, T. Phan, D. Bich, G. Rymski, J. Kohout, V. Chlan, N. Dang, Revealing crucial factors governing magnetic properties of high-energy ball-milled $CoFe_2O_4$ nanoparticles, Ceramics International 51 (2024) 5168–5180. doi.org/10.1016/j.ceramint.2024.11.491.

[105] D. P. Kozlenko, L. S. Dubrovinsky, S. E. Kichanov, E. V. Lukin, V. Cerantola, A. I. Chumakov, B. N. Savenko, Magnetic and electronic properties of magnetite across the high pressure anomaly, Scientific Reports 9 (2019) 4464. doi.org/10.1038/s41598-019-41184-3.

[106] A. Bengtson, D. Morgan, U. Becker, Spin state of iron in Fe_3O_4 magnetite and h–Fe_3O_4, Physical Review B 87 (2013) 155141. doi.org/10.1103/physrevb.87.155141.

[107] D. Levy, V. Diella, M. Dapiaggi, A. Sani, M. Gemmi, A. Pavese, Equation of state, structural behaviour and phase diagram of synthetic $MgFe_2O_4$, as a function of pressure and temperature, Physics and Chemistry of Minerals 31 (2004) 122–129. doi.org/10.1007/s00269-004-0380-4.

[108] E. Greenberg, G. K. Rozenberg, W. Xu, R. Arielly, M. P. Pasternak, A. Melchior, G. Garbarino, L. S. Dubrovinsky, On the compressibility of ferrite spinels: A high-pressure X-ray diffraction study of MFe_2O_4 (M = Mg, Co, Zn), High Pressure Research 29 (2009) 764–779. doi.org/10.1080/08957950903424424.

[109] J. Blasco, G. Subías, J. García, C. Popescu, V. Cuartero, High-pressure transformation in the cobalt spinel ferrites, Journal of Solid State Chemistry 221 (2015) 173–177. doi.org/10.1016/j.jssc.2014.09.028.

[110] M. Merlini, M. Hanfland, M. Gemmi, S. Huotari, L. Simonelli, P. Strobel, Fe^{3+} spin transition in $CaFe_2O_4$ at high pressure, American Mineralogist 95 (2010) 200–203. doi.org/10.2138/am.2010.3347.

[111] G. Radaelli, G. Iannone, M. Marezio, H. Y. Hwang, S.-W. Cheong, J. D. Jorgensen, D. N. Argyriou, Structural effects on the magnetic and transport properties of perovskite $A_{(1-x)}A'_xMnO_3$ (x = 0.25, 0.30), Physical Review B 56 (1997) 8265. https://doi.org/10.1103/PhysRevB.56.8265.